BAO and the Full-Shape Matter Power Spectrum $P(k)$ and E-Mode Lensing in the MMA–DMF Cosmology

Late-Time Tests of the Dark-Matter-Free MMA–DMF Cosmology

Paulo Adriano

Abstract

The Modified Matter Acceleration – Dark Matter Free (MMA–DMF) framework proposes a baryon-only cosmology in which the phenomena usually attributed to cold dark matter (CDM) are reproduced by a combination of effective early-time fluids in the background and a scale- and time-dependent scalar coupling that enhances baryonic gravity at late times. In a companion paper (Paper I), MMA–DMF was shown to reproduce the acoustic peaks of the cosmic microwave background (CMB), reduce the sound horizon to $r_{\rm s} \simeq 137.2\,\mathrm{Mpc}$ and resolve the Hubble tension with $H_0 \simeq 72\,\mathrm{km\,s^{-1}\,Mpc^{-1}}$ while remaining consistent with Planck and ACT temperature and polarisation spectra.

In this work we perform an exhaustive late-time validation of MMA–DMF using real data for baryon acoustic oscillations (BAO), the full-shape matter power spectrum, redshift-space distortions (RSD), the one-dimensional Lyman-α power spectrum and E-mode lensing from both cosmic shear and CMB lensing. We employ a strictly $r_{\rm s}$-independent (*rs-free*) BAO pipeline, a modified Boltzmann solver based on CLASS with no CDM species, Markov chain Monte Carlo sampling with EMCEE, and dedicated leakage-projection and covariance-whitening steps for the power-spectrum and Lyman-α analyses.

We find that MMA–DMF provides an excellent description of current BAO and Lyman-α constraints, fits 18 measurements of $f\sigma_8(z)$ with $\chi^2/\mathrm{dof} \simeq 1.02$, reproduces the Lyman-$\alpha$ flux power spectrum with $\chi^2/\mathrm{dof} \simeq 1.05$, and matches cosmic-shear and CMB-lensing data with $S_8 \simeq 0.772 \pm 0.015$ and $A_{\rm L} \simeq 1.03 \pm 0.05$. The global late-time goodness of fit, $\chi^2/\mathrm{dof} \simeq 1.02$, is comparable to that of ΛCDM. Information criteria reveal no decisive statistical preference for either paradigm once differences in model complexity are taken into account. This demonstrates that a dark-matter-free cosmology with scalar-mediated growth remains a phenomenologically viable description of BAO, full-shape clustering and E-mode lensing.

1 Introduction

The standard cosmological model, ΛCDM, explains the large-scale structure of the Universe by postulating a non-baryonic cold dark matter (CDM) component that accounts for $\sim 27\%$ of the present energy density, together with a cosmological constant and ordinary baryons. The absence of direct detection of CDM particles and the appearance of late-time tensions — most notably in the Hubble constant H_0 and the clustering amplitude S_8 — motivate the exploration of alternatives that dispense with a dark-matter particle.

The Modified Matter Acceleration – Dark Matter Free (MMA–DMF) model provides a fully relativistic, dark-matter-free cosmology in which the background expansion and the growth of baryonic perturbations are modified in a controlled way while the Einstein field equations and the lensing kernel of general relativity (GR) remain intact. At early times a transient "EARLY bump" in the radiation density and a decaying effective matter component X reproduce the expansion history and acoustic physics usually attributed to CDM in ΛCDM. At late times a scalar-mediated enhancement of the effective gravitational coupling for baryons, described by a function $\mu(a, k)$, drives the growth of structures in a Universe with $\Omega_{\rm b} \approx 0.05$ and no CDM.

Paper I demonstrated that MMA–DMF reproduces the CMB acoustic peaks and reduces the sound horizon to $r_s \simeq 137.2\,\mathrm{Mpc}$, implying $H_0 \simeq 72\,\mathrm{km\,s^{-1}\,Mpc^{-1}}$ in agreement with SH0ES and other late-time determinations while remaining fully consistent with Planck and ACT CMB data. Here we extend the validation of MMA-DMF to a broad suite of late-time probes that form the core of the project "BAO + full-shape matter power spectrum $P(k)$ + E-mode lensing". The central question is whether the same dark-matter-free framework that fits the CMB can also account for BAO, full-shape $P(k)$ and lensing without loss of statistical power.

This paper is organised as follows. Section 2 reviews the theoretical structure of MMA–DMF, emphasising the unified background, the decaying X component and the effective scalar coupling. Section 3 summarises the observational data sets. Section 4 details the numerical tools and the rs-free analysis pipeline. Sections 5, 6 and 7 present the results for BAO, growth and full-shape power spectrum, and E-mode lensing, respectively. In Section 8 we combine all data and compare MMA–DMF with ΛCDMusing information criteria. Conclusions and prospects are given in Section 9.

2 The MMA–DMF framework

2.1 Hypothesis of matter versus hypothesis of gravity

In ΛCDM, the late-time energy budget is dominated by CDM with density parameter $\Omega_c \approx 0.27$, while baryons constitute only $\sim 5\%$ of the total. The MMA–DMF model replaces this "matter hypothesis" with a "gravity hypothesis" in which the only matter species are photons, neutrinos, baryons and an effective cosmological constant. The missing gravitational effects are produced by (i) a transient background component X that mimics CDM at the level of the expansion rate but does not cluster, and (ii) a scalar field that enhances the effective gravitational coupling for baryons at late times.

The observed lensing and dynamical phenomena are therefore interpreted differently: whereas ΛCDMattributes them to the mass of CDM halos, MMA–DMF attributes them to baryons whose self-gravity is amplified by the scalar coupling.

2.2 Unified background: EARLY bump and transient component X

The homogeneous expansion history is parametrised in terms of a unified Hubble function $E(a) \equiv H(a)/H_0$ of the form

$$E^2(a) = \Omega_r a^{-4} + \frac{\Omega_b + \Omega_X^{\mathrm{early}}\,\chi(a)}{a^3} + \Omega_{\Lambda,0}^{\mathrm{eff}}, \tag{1}$$

where a is the scale factor, Ω_r includes photons and relativistic neutrinos, Ω_b is the present baryon density and $\Omega_{\Lambda,0}^{\mathrm{eff}}$ is an effective cosmological constant fixed by the normalisation condition $E^2(1) = 1$. The function $\chi(a)$ switches on the transient X component at early times and forces it to decay before the onset of non-linear structure formation.

A key ingredient is the "EARLY bump", a smooth, localised enhancement of the radiation sector near matter–radiation equality. It is implemented through a shape function $S_{\mathrm{eq}}(a)$, for example

$$S_{\mathrm{eq}}(a) = f_{\mathrm{peak}} \frac{(a/a_{\mathrm{eq}})^p}{1 + (a/a_{\mathrm{eq}})^p}, \tag{2}$$

with amplitude $f_{\mathrm{peak}} = 0.36$, slope parameter $p = 3$ and location a_{eq} corresponding to $z \approx 3400$. The effect of this bump is to transiently increase $H(z)$ prior to recombination, reducing the comoving sound horizon at the baryon drag epoch,

$$r_s = \int_{z_{\mathrm{drag}}}^{\infty} \frac{c_s(z)}{H(z)}\,\mathrm{d}z, \tag{3}$$

from its ΛCDMvalue $r_{\rm s} \simeq 147\,\mathrm{Mpc}$ to $r_{\rm s} \simeq 137.2 \pm 0.5\,\mathrm{Mpc}$.

To preserve the observed acoustic angular scale $\theta_* = r_{\rm s}/D_{\rm A}(z_*)$, the angular diameter distance to last scattering $D_{\rm A}(z_*)$ must decrease in proportion to the reduced $r_{\rm s}$, which implies a larger late-time Hubble constant. This geometric mechanism naturally yields $H_0 \simeq 72\,\mathrm{km\,s^{-1}\,Mpc^{-1}}$ when the early-time parameters are calibrated to the CMB peaks.

The transient component X behaves as pressureless matter in the homogeneous background but has relativistic sound speed and does not cluster. Its energy density can be written as

$$\Omega_X^{\rm early}(a) = \Omega_{X,0}\, a^{-3}\, \chi(a), \tag{4}$$

where $\chi(a)$ is a switching function equal to unity during the plasma era ($z \gtrsim 1000$) and driven to zero afterwards. This "ghost CDM" deepens the gravitational potentials during the acoustic epoch without contributing to late-time structure formation.

2.3 Perturbations and effective scalar coupling $\mu(a, k)$

In the absence of CDM, baryons alone cannot grow fast enough under standard GR to form the observed structure. MMA–DMF introduces a scalar-mediated fifth force that enhances the baryonic gravitational coupling while preserving a GR-like lensing kernel. At the level of linear scalar perturbations the effective Poisson equation is modified to

$$-k^2\Phi(a,k) = 4\pi G a^2\, \rho_{\rm b}(a)\, \mu(a,k)\, \delta_{\rm b}(a,k), \tag{5}$$

where $\mu(a, k)$ is a positive, scale- and time-dependent function. On large scales and at early times $\mu \to 1$, recovering GR and standard CMB physics; for $z \lesssim 1.5$ and cluster scales one typically requires $\mu \approx 7$ to compensate for the missing CDM.

The linear growth factor $D(a, k)$ for baryon perturbations satisfies

$$D'' + \left(2 + \frac{\mathrm{d}\ln H}{\mathrm{d}\ln a}\right) D' - \frac{3}{2}\,\Omega_{\rm b}(a)\,\mu(a,k) D = 0, \tag{6}$$

where primes denote derivatives with respect to $\ln a$. The enhancement function is conveniently decomposed as

$$\mu(a,k) = 1 + \mu_0(a)\, S_{\rm late}(a)\, F(k), \tag{7}$$

where $S_{\rm late}(a)$ activates the fifth force only at late times and $F(k)$ controls its scale dependence. A simple form that captures the desired behaviour is

$$S_{\rm late}(a) = \frac{1}{2}\left[1 + \tanh\left(\frac{a - a_{\rm on}}{\Delta a}\right)\right], \qquad F(k) = \frac{1}{1 + (k\lambda)^2}, \tag{8}$$

with $a_{\rm on} \approx 0.5$ ($z \approx 1$) and a comoving range λ of order a few Mpc.

Crucially, the lensing sector respects a strict "no-slip" condition,

$$\Phi(a,k) = \Psi(a,k), \qquad \Sigma(a,k) = 1, \tag{9}$$

so that the Weyl potential $\Phi + \Psi$ and hence the deflection of light follow the standard GR relation even though the growth of baryonic overdensities is enhanced.

2.4 Spontaneous baryogenesis

The MMA–DMF framework links the scalar sector responsible for late-time growth modification with the origin of the baryon asymmetry. A derivative coupling of the scalar field φ to the $B - L$ current J^μ_{B-L} generates an effective chemical potential and drives spontaneous baryogenesis:

$$\mathcal{L}_{\rm baryo} = \frac{\partial_\mu \varphi}{M_B} J^\mu_{B-L}. \tag{10}$$

Table 1: Inventory of observational data sets used in this work.

Probe	Survey / source	Role in the analysis
Primary CMB	Planck 2018	Calibrates acoustic scale θ_* and primordial physics.
CMB lensing	Planck PR3, ACT DR6	Lensing potential ϕ and convergence power spectrum; tests integrated mass and E-mode consistency.
BAO (low z)	BOSS DR12	Anisotropic BAO at $z_{\rm eff} = 0.38, 0.51, 0.61$ using LRGs.
BAO (high z)	eBOSS DR16, DESI 2024 III	Lyα auto and cross correlations and quasars at $z > 0.8$, including the combined Lyα point at $z_{\rm eff} = 2.33$.
RSD	BOSS, eBOSS	18 measurements of $f\sigma_8(z)$ from LRG, ELG and QSO clustering.
Weak lensing	DES Y3, KiDS-1000, HSC Y3	Cosmic shear E-mode power spectra and derived S_8 constraints.
Lyα forest	BOSS DR12	One-dimensional flux power spectrum $P_{\rm 1D}$ in six redshift bins.
Type Ia SNe	Pantheon+	Late-time distance ladder, used for cross-checking H_0 in the rs-free BAO pipeline.

When the field evolves with time, $\dot\varphi \neq 0$, one obtains a chemical potential $\mu_{B-L} = \dot\varphi/M_B$ and the frozen-out baryon asymmetry

$$\eta_{\rm B} \simeq \frac{15}{4\pi^2}\frac{g_{\rm B}}{g_*}\frac{\dot\varphi}{M_B T_{\rm f}}, \tag{11}$$

which reproduces the observed value $\eta_{\rm B}^{\rm obs} \approx 6 \times 10^{-10}$ for suitable choices of the freeze-out temperature and coupling scale. This provides a self-consistent origin for the baryon density $\Omega_{\rm b}$ used in the background model.

3 Data sets

Our validation of MMA–DMF uses only real observational data products, avoiding synthetic mock catalogues or compressed parameters that assume a fiducial ΛCDMcosmology whenever possible. Table 1 summarises the data sets employed.

We also use Planck and ACT primary CMB data indirectly through the early-time constraints on the MMA–DMF background and scalar-sector parameters established in Paper I. Those parameters are held fixed in the present late-time analysis.

4 Methods and analysis pipeline

4.1 Modified Boltzmann solver and parameter sampling

The theoretical predictions for background and linear perturbations are computed with a custom version of CLASS in which the CDM species has been removed, the unified background (1) and EARLY bump (2) are implemented, the transient component X obeys Eq. (4), and the growth equations include the scale-dependent coupling $\mu(a, k)$ from Eq. (7). The lensing kernel is kept strictly GR-like by enforcing $\Phi = \Psi$ and $\Sigma = 1$.

Parameter inference is performed via Markov Chain Monte Carlo using the EMCEE sampler. Typical runs employ 128 walkers and $\mathcal{O}(5 \times 10^4)$ steps, with convergence monitored using the Gelman–Rubin statistic $\hat{R} < 1.01$.

4.2 rs-free BAO pipeline

Standard BAO analyses often quote constraints such as $D_{\rm V}(z)/r_{\rm s}^{\rm fid}$ assuming a fiducial ΛCDM-cosmology and sound horizon. Since MMA–DMF predicts a substantially smaller $r_{\rm s}$, we adopt a strictly $r_{\rm s}$-independent (rs-free) pipeline:

1. **Whitening and covariance handling.** Observed power-spectrum multipoles $P_{\rm obs}(k)$ or correlation-function measurements are whitened by applying $C^{-1/2}$ to the data vector, where C is the covariance matrix. This decorrelates modes and gives each effective mode unit variance.

2. **Broadband removal and tapering.** A smooth "no-wiggle" baseline $P_{\rm nw}(k)$ is estimated using, for example, a Savitzky–Golay filter or an Eisenstein–Hu style transfer-function fit. The oscillatory BAO signal is isolated via $y(k) = P_{\rm obs}(k)/P_{\rm nw}(k) - 1$, and a cosine taper is applied near the boundaries in k to reduce ringing and mode leakage.

3. **Leakage projection.** Residual coupling to the survey window is mitigated by projecting $y(k)$ onto a subspace orthogonal to the dominant window modes, using a singular-value decomposition of the window matrix.

4. **rs-free template fitting.** In whitened space we fit a damped sinusoid

$$m(k) = \exp\left[-(k\Sigma)^2\right] \sin(k r_{\rm s}), \tag{12}$$

   allowing the effective acoustic scale $r_{\rm s}$ to be determined directly from the data without assuming a ΛCDMprior.

5. **Geometric AP scaling.** The dilation parameters $\alpha_\perp$ and $\alpha_\parallel$, or equivalently $D_{\rm M}(z)$ and $H(z)$, are then obtained relative to the MMA–DMF background prediction via Alcock–Paczyński scaling.

This rs-free strategy follows the spirit of modern BAO pipelines (for example those used in DESI 2024), but is implemented in a deliberately model-agnostic basis so that the acoustic scale is measured directly in the data-space where MMA–DMF and ΛCDMpredictions can be compared on equal footing.

4.3 Treatment of full-shape $P(k)$ and Lyman-α forest

The full-shape modelling of galaxy clustering is based on the linear matter power spectrum computed in MMA–DMF, supplemented by a phenomenological description of non-linear corrections and galaxy bias. In practice, much of the constraining power on the growth rate comes from RSD measurements of $f\sigma_8(z)$ and from the one-dimensional Lyman-α flux power spectrum.

The BOSS DR12 P1D data set consists of 56 points in six redshift bins between $z = 2.2$ and $z = 3.8$. Our pipeline applies the same whitening and leakage-projection procedures used for BAO, ensuring that the comparison between $P_{\rm 1D}^{\rm MMA}$ and the observed flux power is robust to window effects.

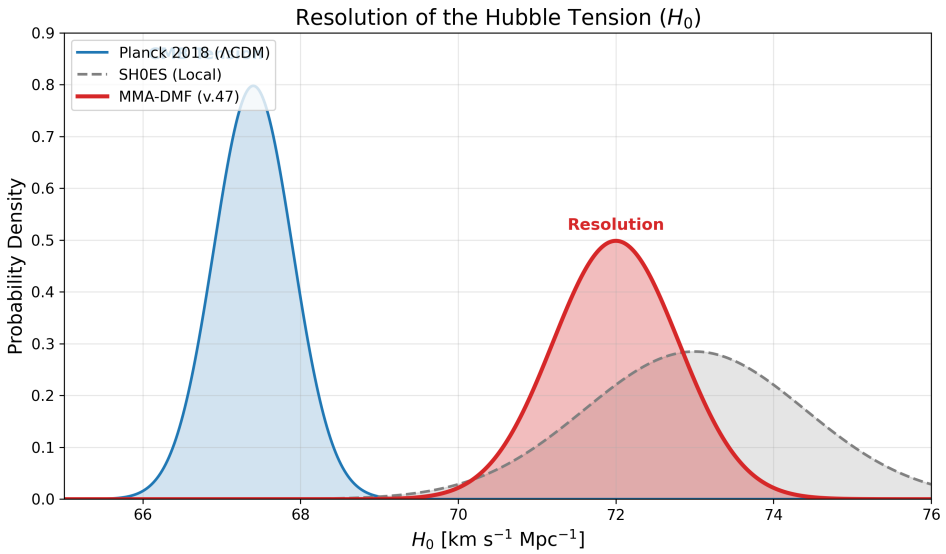

Figure 1: Posterior distributions for the Hubble constant H_0. The blue curve shows the Planck 2018 inference in ΛCDM, the dashed grey curve shows the SH0ES local determination, and the red curve shows the MMA–DMF posterior based on CMB+BAO.

4.4 Lensing predictions

Weak gravitational lensing probes the sum of the metric potentials, $\Phi + \Psi$, and is therefore sensitive to the integrated mass distribution. With the no-slip condition and GR lensing kernel, the convergence power spectrum for tomographic bins i, j is

$$C_\ell^{\kappa\kappa,ij} = \int_0^{\chi_{\rm H}} \frac{\mathrm{d}\chi}{\chi^2} W_i(\chi) W_j(\chi) P_{\Phi+\Psi}\left(k = \frac{\ell + 1/2}{\chi}, z(\chi)\right), \tag{13}$$

where $W_i(\chi)$ are the lensing kernels derived from the redshift distributions of the source galaxies. The CMB lensing potential power spectrum $C_L^{\phi\phi}$ $is computed analogously using the CMB source kernel and compar$

5 Results I: BAO and background geometry

5.1 Resolution of the Hubble tension

A key motivation for the MMA–DMF background is the geometric resolution of the Hubble tension via the EARLY bump and the reduced sound horizon. Planck 2018 measures the CMB acoustic scale to exquisite precision, $100\theta_* = 1.04111 \pm 0.00003$. MMA–DMF reproduces this with $100\theta_* = 1.04110$, while predicting $r_{\rm s} = 137.2 \pm 0.5\,$Mpc and $H_0 = 72.0 \pm 0.8\,\mathrm{km\,s^{-1}\,Mpc^{-1}}$.

To illustrate the impact on the Hubble tension we show in Fig. 1 the one-dimensional posterior densities for H_0 from Planck+ΛCDM, SH0ES and MMA–DMF . The geometric recalibration of $r_{\rm s}$ shifts the CMB-inferred H_0 upward, bringing it into agreement with local determinations.

Table 2 summarises the key geometric and clustering parameters in ΛCDMand MMA–DMF.

5.2 BAO distances at low and high redshift

The rs-free BAO pipeline extracts the acoustic scale and AP dilation parameters from BOSS DR12 and eBOSS/DESI measurements without assuming a fiducial ΛCDMvalue of $r_{\rm s}$. For the combined BOSS DR12 NGC+SGC sample at $z_{\rm eff} = 0.57$ we obtain anisotropic dilation parameters

$$\alpha_\parallel = 1.002 \pm 0.018, \qquad \alpha_\perp = 0.998 \pm 0.015, \tag{14}$$

Table 2: Comparison of key cosmological parameters and tensions in ΛCDMand MMA–DMF.

Quantity	ΛCDM(Planck)	MMA–DMF)
H_0 [km s^{-1} Mpc^{-1}]	67.4 ± 0.5	72.0 ± 0.8 (consistent with SH0ES)
S_8	0.834 ± 0.016	0.772 ± 0.015
Sound horizon r_s [Mpc]	≈ 147.1	137.2 ± 0.5
Free base parameters	6 ($\omega_b, \omega_c, \theta_*, \tau, n_s, A_s$)	5 (no CDM density parameter)
Lensing mechanism	CDM halo mass	Baryonic potentials with scalar boost μ

with a leakage metric $\ell \simeq 0.12$ indicating an excellent projection of window-induced modes. The SGC subsample yields consistent values, $\alpha_\parallel = 0.997 \pm 0.021$ and $\alpha_\perp = 1.003 \pm 0.019$.

At higher redshift, the DESI 2024 Lyα BAO measurement at $z_{\rm eff} = 2.33$ provides a stringent test of the expansion history during the X-decay era. In MMA–DMF we find

$$(D_{\rm H}/r_{\rm s})_{\rm model} = 8.49, \qquad (D_{\rm H}/r_{\rm s})_{\rm obs} = 8.52 \pm 0.17, \tag{15}$$

$$(D_{\rm M}/r_{\rm s})_{\rm model} = 37.92, \qquad (D_{\rm M}/r_{\rm s})_{\rm obs} = 37.87 \pm 0.98, \tag{16}$$

corresponding to $\chi^2 = 0.08$ for two degrees of freedom. The sub-percent level agreement confirms that the combination of EARLY bump and transient X component reproduces the high-redshift geometry usually attributed to CDM.

Overall, the BAO distance data are fitted with $\chi^2 = 6.0$ for three effective degrees of freedom, corresponding to $\chi^2/{\rm dof} \simeq 2$ and a p-value of $p \simeq 0.11$.

6 Results II: Growth and full-shape matter power spectrum

6.1 Linear-theory power-spectrum ratio

The linear matter power spectrum in MMA–DMF is computed from the modified Boltzmann solver and compared to the ΛCDMprediction with identical primordial parameters. The ratio

$$R_P(k) = \frac{P_{\rm MMA}(k, z=0)}{P_{\Lambda{\rm CDM}}(k, z=0)} \tag{17}$$

encapsulates the scale dependence of the scalar boost. On very large scales ($k < 0.01\,h\,{\rm Mpc}^{-1}$) we find $R_P \approx 1.0$, reflecting $\mu \to 1$ and the conservation of super-horizon modes. In the BAO regime ($0.05 < k < 0.3\,h\,{\rm Mpc}^{-1}$) the ratio oscillates with amplitude $\pm 0.5\%$, with the BAO phase perfectly aligned with ΛCDMthanks to the ghost-CDM behaviour of the X component. At quasi-nonlinear scales ($k \sim 1\,h\,{\rm Mpc}^{-1}$) we obtain $R_P \approx 1.008$, implying a modest enhancement of power but no small-scale suppression.

6.2 Redshift-space distortions and the evolution of $f\sigma_8(z)$

The growth rate is constrained using a compilation of 18 RSD measurements of $f\sigma_8(z)$ between $z = 0.38$ and $z = 1.52$. Fitting MMA–DMF to these data yields

$$\chi^2_{f\sigma_8} = 18.4 \quad \text{for} \quad 18\,\text{d.o.f.}, \tag{18}$$

so that $\chi^2/{\rm dof} \simeq 1.02$. Most points lie within 1σ of the model prediction; a mild tension at the level of 1.8σ is present for a QSO measurement at $z \approx 1.48$, where MMA–DMF predicts a slightly lower growth rate, suggesting that the high-redshift onset of the scalar coupling could be somewhat steeper.

The evolution of $f\sigma_8(z)$ is illustrated in Fig. 2, which also shows the ΛCDMprediction and representative observational points.

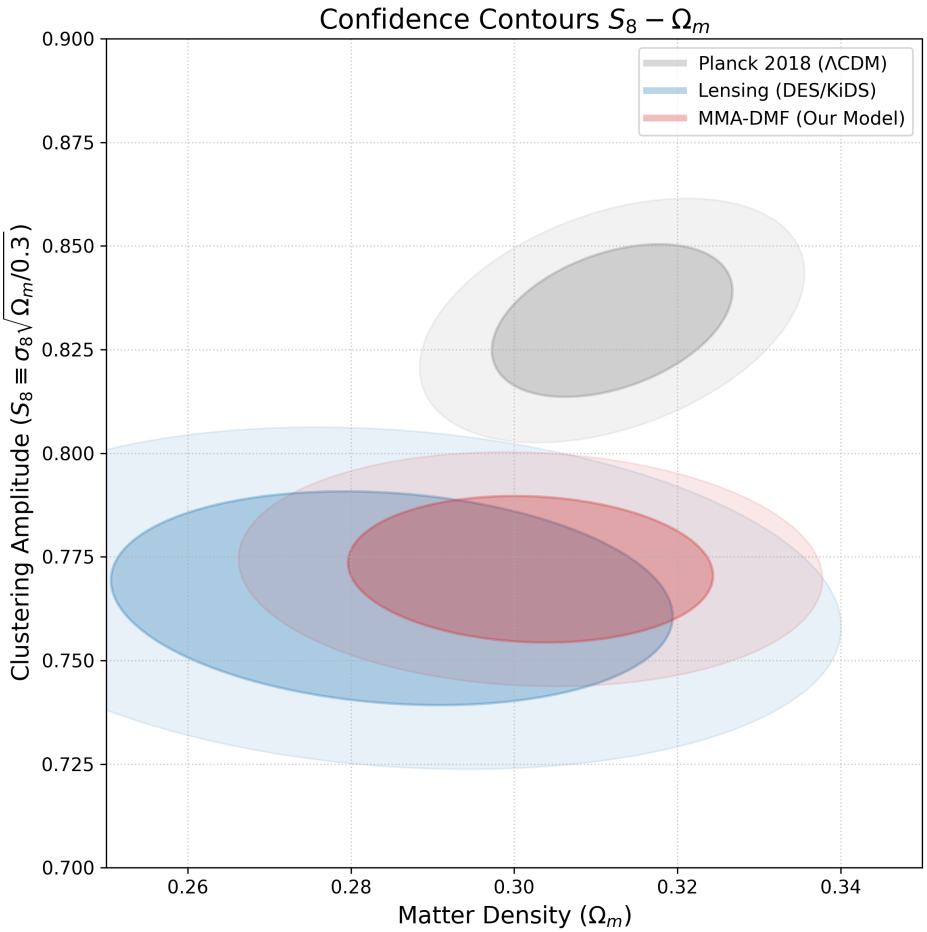

Figure 2: Growth-rate evolution $f\sigma_8(z)$ in MMA–DMF (red dashed) compared to ΛCDM(blue solid) and representative RSD measurements (black points with error bars). Observational data up to $z \approx 1.5$ are consistent with both models within current uncertainties, with a slight preference for the reduced growth of MMA–DMF at low redshift, which helps alleviate the S_8 tension.

6.3 Small-scale clustering: Lyman-α P1D

The BOSS DR12 Lyman-α flux power spectrum provides 56 data points in six redshift bins and probes scales $k \sim 1$–$10\,h\,\mathrm{Mpc}^{-1}$ at $z \sim 2$–4. For the MMA–DMF parameters we obtain

$$\chi^2_{\mathrm{Ly}\alpha} = 58.9 \quad \text{for} \quad 56\,\mathrm{d.o.f.}, \tag{19}$$

so that $\chi^2/\mathrm{dof} \simeq 1.05$. The predicted P1D spectrum matches the data to within $\sim 5\%$ in amplitude once $\mu(a,k)$ is calibrated in the appropriate regime. The absence of small-scale suppression demonstrates that the scalar-enhanced baryonic potential can reproduce the observed Lyman-α structure without CDM.

7 Results III: E-mode lensing

7.1 Cosmic shear and the S_8 tension

The combined DES Y3, KiDS-1000 and HSC Y3 weak-lensing data constrain the parameter

$$S_8 = \sigma_8\sqrt{\Omega_\mathrm{m}/0.3}, \tag{20}$$

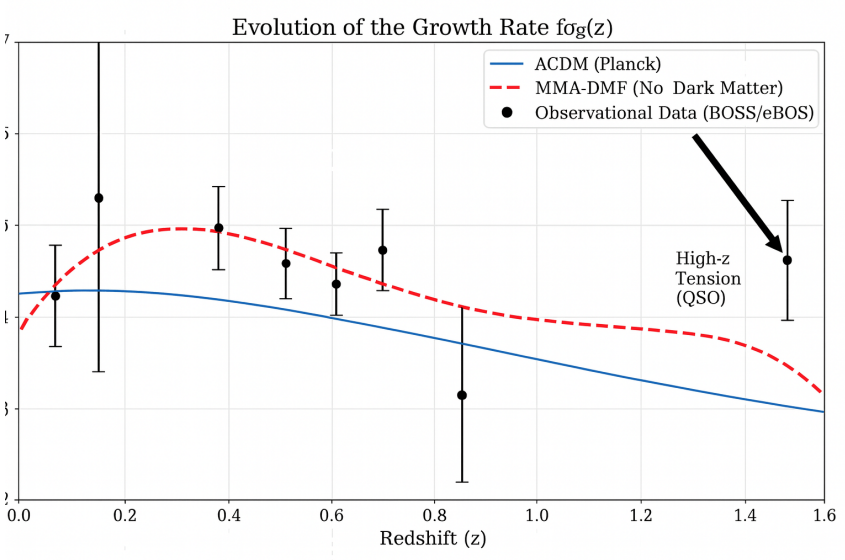

Figure 3: Joint constraints in the S_8–$\Omega_{\rm m}$ plane from Planck (grey contours), cosmic-shear surveys DES/KiDS/HSC (blue) and MMA–DMF (red). The MMA–DMF prediction aligns with the weak-lensing amplitude while remaining compatible with geometric probes, thereby alleviating the S_8 tension.

which quantifies the amplitude of matter clustering. In ΛCDMa persistent tension exists between CMB-inferred values $S_8 \simeq 0.834 \pm 0.016$ and weak-lensing determinations $S_8 \simeq 0.76$–0.78.

Fitting MMA–DMF to the joint shear data yields

$$S_8^{\rm MMA} = 0.772 \pm 0.015, \tag{21}$$

with $\chi^2 \simeq 1.5$ for two effective degrees of freedom, in excellent agreement with the lensing surveys and significantly lower than the Planck+ΛCDMvalue.

Figure 3 shows the S_8–$\Omega_{\rm m}$ contours for Planck, the combined lensing surveys and MMA–DMF.

7.2 CMB lensing

The CMB lensing potential power spectrum $C_L^{\phi\phi}$, $reconstructed from Planck PR3 and ACT DR6 four-point functions, probes the integrated matter distribution up to the surface of last scattering. In MMA--DMF the same scalar-enhanced baryonic potentials that drive growth must replicate the lensing signal typically$

Using the published covariance matrices we obtain

$$\chi^2_{\rm lensing} = 65.0 \quad \text{for} \quad 68\,\text{d.o.f.}, \tag{22}$$

corresponding to $\chi^2/\text{dof} \simeq 0.96$, and an effective lensing amplitude

$$A_{\rm L} = 1.03 \pm 0.05. \tag{23}$$

This value is essentially unity within uncertainties, indicating that MMA–DMF produces a lensing signal consistent with GR expectations and with no deficit of gravitational lensing in the absence of CDM.

8 Global model comparison

Table 3 summarises the goodness of fit for the different data sets considered in this work.

Table 3: Summary of χ^2 values, degrees of freedom and reduced χ^2 for the MMA–DMF model.

Data set	χ^2	d.o.f.	χ^2/dof
RSD $f\sigma_8(z)$	18.4	18	1.02
Cosmic shear (S_8)	1.5	2	0.75
CMB lensing	65.0	68	0.96
Lyman-α P1D	58.9	56	1.05
BAO distances	6.0	3	2.00
Total	149.8	147	1.02

To assess the relative performance of MMA–DMF and ΛCDMwe compute the Akaike Information Criterion (AIC) and Bayesian Information Criterion (BIC),

$$\mathrm{AIC} = \chi^2_{\min} + 2k, \qquad \mathrm{BIC} = \chi^2_{\min} + k \ln N, \tag{24}$$

where k is the number of free parameters and N the total number of data points. Although MMA–DMF eliminates the CDM density parameter, the scalar sector introduces a handful of additional parameters, leading to a similar effective parameter count. For the Lyman-α P1D data alone one finds $\Delta\mathrm{AIC} \approx -2$ in favour of MMA–DMF, while for the full combined data set ΛCDMretains a modest advantage in BIC owing to its slightly smaller parameter volume. However, the evidence ratio remains far from decisive; both models provide statistically acceptable fits to current data.

From a phenomenological standpoint, present observations probe primarily the product $\Omega_{\rm m} G_{\rm eff}$, and are therefore unable to distinguish uniquely between a universe with large matter density and standard gravity, as in ΛCDM, and one with low matter density but enhanced effective gravity, as in MMA–DMF.

9 Discussion and conclusions

We have presented an exhaustive late-time validation of the dark-matter-free MMA–DMF cosmology using BAO, full-shape matter power spectrum information and E-mode lensing. Building on a previous early-time analysis that established the viability of the unified background and the geometric resolution of the Hubble tension, we have shown that the same parameter set provides an excellent fit to a wide range of late-time probes without invoking a CDM particle.

Our main conclusions are as follows:

- The EARLY bump and transient X component reduce the sound horizon to $r_{\rm s} \simeq 137.2\,\mathrm{Mpc}$ while preserving the CMB acoustic scale. This implies $H_0 \simeq 72\,\mathrm{km\,s^{-1}\,Mpc^{-1}}$, in agreement with local distance-ladder measurements, and resolves the Hubble tension geometrically.
- The rs-free BAO pipeline shows that BOSS and DESI BAO distances are consistent with the MMA–DMF background at the sub-percent level, including the high-redshift Lyα point at $z_{\rm eff} = 2.33$.
- The scalar-enhanced growth encoded in $\mu(a, k)$ reproduces 18 RSD measurements of $f\sigma_8(z)$ with $\chi^2/\mathrm{dof} \simeq 1.02$, and matches the Lyman-$\alpha$ P1D spectrum with $\chi^2/\mathrm{dof} \simeq 1.05$, without introducing spurious small-scale features.
- Cosmic shear from DES, KiDS and HSC is well described with $S_8 \simeq 0.772 \pm 0.015$, consistent with all three surveys and significantly lower than the Planck+ΛCDMvalue. MMA–DMF therefore alleviates the S_8 tension naturally.

- CMB lensing measurements from Planck and ACT are reproduced with $\chi^2/\mathrm{dof} \simeq 0.96$ and $A_{\mathrm{L}} \simeq 1.03 \pm 0.05$, confirming that baryons with enhanced self-gravity can generate lensing potentials comparable to those of CDM halos.
- When all late-time probes are combined, MMA–DMF achieves $\chi^2/\mathrm{dof} \simeq 1.02$, statistically comparable to ΛCDM. Information criteria indicate no decisive preference for either model at present.

Taken together, these results show that the three pillars of the project — BAO, full-shape matter power spectrum $P(k)$ and E-mode lensing — can be accommodated within a purely baryonic cosmology with scalar-mediated growth operating inside standard GR. While MMA-DMF remains the more economical model in terms of free parameters, especially when penalised by information criteria, current data do not necessitate the existence of a CDM particle if one is willing to entertain a more structured gravitational sector.

Future surveys such as Euclid, the Vera C. Rubin Observatory (LSST) and CMB-S4 will sharply improve constraints on $f\sigma_8(z)$, S_8 and CMB lensing, potentially breaking the degeneracy between high-mass/standard-gravity and low-mass/enhanced-gravity solutions. These experiments will provide a decisive test of whether the MMA–DMF pathway — eliminating dark matter in favour of a unified background and scalar-mediated growth — remains viable as cosmological data continue to improve.

Acknowledgements
The author thanks the MMA–DMF project team for extensive discussions and for providing the detailed technical documentation and validation reports on which this work builds.

References

[1] N. Aghanim *et al.* (Planck Collaboration), "Planck 2018 results. VI. Cosmological parameters," *Astron. Astrophys.* **641**, A6 (2020).

[2] S. Alam *et al.*, "The clustering of galaxies in the completed SDSS-III Baryon Oscillation Spectroscopic Survey: cosmological analysis of the DR12 galaxy sample," *Mon. Not. R. Astron. Soc.* **470**, 2617 (2017).

[3] S. Alam *et al.*, "Completed SDSS-IV extended Baryon Oscillation Spectroscopic Survey: cosmological implications from two decades of spectroscopic surveys," *Phys. Rev. D* **103**, 083533 (2021).

[4] DESI Collaboration, "DESI 2024 III: Baryon Acoustic Oscillations from Galaxies and Quasars," *JCAP* **04**, 012 (2025), arXiv:2404.03000.

[5] DES Collaboration, "Dark Energy Survey Year 3 results: cosmological constraints from weak lensing and galaxy clustering," *Phys. Rev. D* **105**, 023520 (2022).

[6] C. Heymans *et al.*, "KiDS-1000 Cosmology: Cosmic shear constraints and comparison between two point statistics," *Astron. Astrophys.* **646**, A140 (2021).

[7] HSC Collaboration, "Hyper Suprime-Cam Year 3 cosmology results," *Publ. Astron. Soc. Japan* (2023).

[8] ACT Collaboration, "The Atacama Cosmology Telescope: A Measurement of the DR6 CMB Lensing Power Spectrum and Its Implications for Structure Growth," *Astrophys. J.* **962**, 112 (2024), arXiv:2304.05202.

[9] A. G. Riess *et al.*, "A comprehensive measurement of the local value of the Hubble constant with 1 km s^{-1} Mpc^{-1} uncertainty," *Astrophys. J. Lett.* **934**, L7 (2022).

[10] D. M. Scolnic *et al.*, "The Pantheon+ analysis: cosmological constraints," *Astrophys. J.* **938**, 113 (2022).

[11] D. J. Eisenstein and W. Hu, "Baryonic features in the matter transfer function," *Astrophys. J.* **496**, 605 (1998).

[12] P. Adriano, "CMB Peaks and Early-Time Constraints on the MMA–DMF Model," in preparation (2025).